Accelerating Self-Imaging: The Airy-Talbot Effect

Yaakov Lumer, Lee Drori, Yoav Hazan, and Mordechai Segev
Physics Department, Technion—Israel Institute of Technology, Haifa 32000, Israel
(Received 9 March 2015; published 2 July 2015)

We present a new type of self-imaging phenomenon: self-imaging along curved trajectories. Unlike the Talbot effect, where self-imaging occurs for periodic wave patterns propagating along a straight line, here the field is generally not periodic and is self-imaged along curved trajectories. In the paraxial regime, self-imaging along a parabolic trajectory can ideally go on indefinitely. In the nonparaxial regime the self-imaging is along a circular trajectory and lasts as long as the beam bends. We demonstrate this accelerating self-imaging effect experimentally, and discuss generalizations to higher dimensions.

DOI: 10.1103/PhysRevLett.115.013901 PACS numbers: 42.25.-p, 42.30.Va

In the Talbot effect, first observed in 1836 [1], a periodic paraxial optical field pattern self-reproduces itself at constant intervals. The effect was explained by Lord Rayleigh in 1881 [2], who gave the mathematical conditions for the effect, which is also called self-imaging, to occur. The Talbot effect has many manifestation in optics, from interferometry and optical testing [3], to optics in parity-time ($\mathcal{PT}$) symmetric system [4], quantum optics [5], waveguide arrays [6], and high numerical aperture, nonparaxial illumination [3], and can also appear with incoherent light under certain conditions [3,7]. The Talbot effect has also attracted research interest in other physical fields such as matter waves [8,9], plasmons [10], and x-ray phase imaging [11]. Thus far, research on the Talbot effect and self-imaging in general has strictly dealt with self-imaging along a straight propagation line [12–14]. That is, the field is reproduced strictly in the plane normal to the propagation direction. Unrelated to self-imaging, recent years have seen a surge in the study of accelerating beams—optical beams whose trajectory is bent, as a consequence of interference effects. These accelerating beams, first conceived in the context of quantum mechanics in 1979 [15], were introduced into the optical domain in 2007 [16,17] and subsequently attracted much attention [18]. Applications of such accelerating beams include particle manipulation [19,20], imaging and microscopy [21,22], accelerating temporal pulses in dispersive media [23,24] and much more. The acceleration is not limited to small angles: in 2012, self-accelerating wave packets of Maxwell's equations, that is, beams that bend almost all the way to 180°, were predicted [25] and demonstrated soon thereafter [26–28]. Accelerating beams were also shown experimentally with matter waves (a quantum wave packet of a single electron), using an electron microscope [29]. It is therefore natural to ask whether it is possible to have an accelerating self-imaging effect.

Here, we present, theoretically and experimentally, the Airy-Talbot effect: self-imaging of wave packets along accelerated (bent) trajectories. While the concept seems similar to the well-known Talbot effect, the underlying physics is different. Unlike the Talbot effect, the self-imaging accelerating wave packet need not be periodic, but instead can have an almost arbitrary shape and can be described as a sum of fundamental accelerating beams. We present examples in two regimes. The first regime is the paraxial regime, where the fundamental accelerating beams are Airy beams, and the acceleration is on a parabolic trajectory. In this case, the ideal, infinite energy beams can self-image indefinitely, while finite energy beams can self-reproduce a finite number of times, in clear correspondence to the Talbot effect. Following the theoretical part, we also demonstrate the accelerating self-imaging phenomenon in the paraxial regime experimentally. The second regime is the nonparaxial regime, where the fundamental accelerating beams display a half-Bessel-function shape, and the acceleration is along a half circle. In the nonparaxial regime, the self-imaging is azimuthal—the beam self-reproduces along planes of constant angle. As such, self-imaging is fundamentally limited to a finite number of times, depending on the angular distance between the self-reproducing planes. In both regimes, we provide the both the criteria for accelerating self-imaging to occur, and for the period of self-imaging.

The Talbot effect, which is the self-imaging of periodic optical fields, has been studied extensively in various different configurations. It has been generalized to incoherent beams [3] and to the self-imaging of optical fields that are not necessarily periodic [12,13]. In all of these cases, the self-imaging was along a straight line. That is, the optical field reproduces itself at constant intervals, without transversal shifts. In order for the field to self-reproduce along a straight line, its spatial spectrum must be associated with k_z values at constant intervals $k_{z,q} = k_{z,0} - q(2\pi/z_M)$, where $k_{z,0}$ is a positive real constant, q is a natural number, and z_M is the longitudinal period in which the field self-images. The field (ignoring the carrier phase of $k_{z,0}$, and using only one dimension for simplicity) can then be written as $\psi(x,z) = \sum_q a_q(x)\exp(-iq2\pi z/z_M)$, which is

clearly periodic along z with period z_M. In the paraxial regime, this condition can be met by requiring the field to be periodic, meaning that its transverse spatial spectrum contains wave numbers at constant intervals $k_x = mk_{x,0}$, where m is an integer and $k_{x,0}$ is a constant. Then, using the paraxial dispersion relation for a monochromatic field of wavelength λ, $k_z = (\lambda/\pi)k_x^2$, it is clear that the condition on k_z is met. This self-imaging of periodic fields is called the Talbot effect.

In order to generalize the self-imaging phenomenon to curved trajectories, we first move to a reference frame moving along the said trajectory. Let us begin with the paraxial regime, where we start with the paraxial wave equation written in normalized coordinates in one transverse dimension:

$$i\partial_s\psi + \frac{1}{2}\partial_u^2\psi = 0. \tag{1}$$

We move to a frame of reference along a parabolic trajectory by writing $u' = u - \frac{1}{4}s^2$, $s' = s$, and $\psi(u,s) = \phi(u',s')\exp[i(\frac{1}{2})u's' + i(\frac{1}{24})s'^3]$ [30,31], and get the paraxial equation in the accelerating frame of reference

$$i\partial_{s'}\phi - \frac{1}{2}u'\phi + \frac{1}{2}\partial_{u'}^2\phi = 0. \tag{2}$$

The eigenfunctions of Eq. (2) with eigenvalue $\frac{1}{2}\Delta$ are Airy functions, shifted in Δ: $\phi_\Delta(u',s') = \mathrm{Ai}(u'-\Delta)\exp(-\frac{1}{2}i\Delta s')$. An example of such a field, in the original frame of reference, can be seen in Fig. 1(a). Now, in order to find waves that self-image, we seek solutions whose spatial spectrum consists of propagation constants at constant intervals—in an analogous way to the Talbot effect. We find, in the accelerating frame of reference, the general solution

$$\phi(u',s') = \sum_n c_n \mathrm{Ai}(u'-\Delta n)\exp\left(-i\frac{1}{2}n\Delta s'\right), \tag{3}$$

where the c_n are arbitrary coefficients. It is clear that the field in Eq. (3) self-images at constant intervals of $s'_q = (4\pi/\Delta)q$. Moving back the field in Eq. (3) to the original frame of reference, it is now written as

$$\psi(u,s) = \exp\left(-\frac{i}{12}s^3 + \frac{i}{2}us\right) \times \sum_n c_n \mathrm{Ai}\left(u - \Delta n - \left(\frac{s}{2}\right)^2\right)\exp\left(-\frac{1}{2}in\Delta s\right), \tag{4}$$

and the intensity pattern is

$$I(u,s) = \left|\sum_n c_n \mathrm{Ai}\left(u - \Delta n - \left(\frac{1}{2}s\right)^2\right)\exp\left(-\frac{1}{2}is\Delta n\right)\right|^2. \tag{5}$$

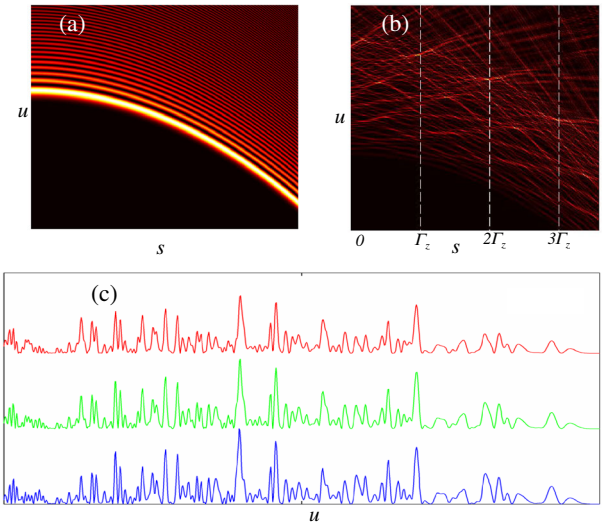

FIG. 1 (color online). (a) Intensity plot of the one-dimensional Airy beam. (b) Intensity plot of the beam of the form of Eq. (4), exhibiting the Airy-Talbot effect. The beam is comprised of an addition of 20 Airy beams, each multiplied by a random coefficient, and shifted along u with $\Delta = 3$, corresponding to a longitudinal periodicity of $\Gamma = 4\pi/3$. (c) Intensity cross sections at three planes of self-imaging, $z = \Gamma$, 2Γ, and 3Γ, marked by dashed lines in (b). The cross sections are shifted along the parabolic trajectory in order to make the comparison clearer.

In other words, at every two planes whose distance is an integer multiple of , the intensity distribution repeats itself, shifted along the parabolic trajectory $u - (\frac{1}{2}s)^2 = \text{const.}$ The field itself self-reproduces up to a global phase factor, as can be seen in Eq. (4). An example of a field with accelerated self-imaging, as described by Eq. (4), is given in Figs. 1(b) and 1(c). Figure 1(b) depicts the intensity pattern for a field comprised of a superposition of 20 Airy beams, shifted with respect to one another, and each multiplied by a different random coefficient. The value of the transversal shift is $\Delta = 3$. In order to visualize the self-imaging property, we plot the field at three planes: $z = \Gamma$, 2Γ, and 3Γ, marked by dashed lines in Fig. 1(b). The three plots are presented in Fig. 1(c), shifted along the parabolic trajectory to align them, making the comparison clearer. It can be clearly seen that despite the seemingly random pattern, the intensity is identical at all three planes. This self-imaging phenomenon repeats indefinitely in the case of ideal, infinite-power Airy beams. If we use finite power Airy beams, the self-imaging persists as long as the beam maintains its shape-preserving self-accelerating properties. Hence, thus far we have presented self-imaging of nonperiodic paraxial fields that self-reproduce along parabolic trajectories.

An alternative way to achieve the result of Eq. (4) is to look at a field whose spatial spectrum is an arbitrary periodic function $g(k)$ such that $g[k + (2\pi/\Delta)] = g(k)$:

$$\tilde{\phi}(k) = g(k) = \sum_n c_n \exp(-ikn\Delta). \tag{6}$$

The field in Eq. (6), if we choose to treat the Fourier plane as $s = 0$ (which can be easily done with a lens), self-images according to the Talbot effect. Now, we superimpose on the field a cubic phase factor of $\exp(\frac{1}{3}ik^3)$, which is known to cause self-acceleration after the Fourier transform [16,30], meaning the spatial spectrum of our field is now

$$\tilde{\phi}(k) = \exp\left(\frac{1}{3}ik^3\right)\sum_n c_n \exp(-ikn\Delta). \tag{7}$$

Fourier transforming the spatial spectrum in Eq. (7), we can write

$$\psi(u,0) = \mathcal{F}\{\tilde{\phi}\} = \sum_n c_n \mathrm{Ai}(u - \Delta n). \tag{8}$$

By propagating the field in Eq. (8) to any $s > 0$ we can immediately get the result in Eq. (4).

We now demonstrate the paraxial Airy-Talbot effect experimentally. In this case, it is most convenient to use the formalism presented in Eq. (7) to generate accelerating self-imaging beams with nonperiodic fields. In the experiment we demonstrate accelerated self-imaging in one transversal dimension. We generate an Airy beam by using a spatial light modulator (SLM), which imposes a cubic phase on the beam. To create the Airy-Talbot beam, we choose the periodic function g such that it is a pure phase: $g = \exp(i\gamma)$. Thus, the overall phase imposed by the SLM is

$$\varphi(x_s) = \frac{1}{3}d_0^3 x_s^3 + \gamma(x_s). \tag{9}$$

Here, x_s is the coordinate on the SLM and $\gamma(x_s) = \gamma(x_s + D)$. Using a lens with focal length f, the beam at plane $z = 0$ is the Fourier transform of a field with a phase profile described in Eq. (9), and can be written as

$$\psi(x) = \sum_n c_n \mathrm{Ai}\left(\frac{x}{x_0} - \Delta n\right), \tag{10}$$

where $x_0 = d_0 D f/2\pi$ and $\Delta = 2\pi/d_0 D$. In our experiment, we use $f = 250$ mm, $D = 0.9$ mm, and $d_0 = 2.3$ mm^{-1} with wavelength $\lambda = 532$ nm. A sketch of the experimental system is plotted in Fig. 2(a). In our case, the period is $\Gamma = 115$ mm. Figure 2(b) shows a side view of the intensity profile, and Fig. 2(c) presents the cross sections at three different planes. Because of the intensity attenuation originating from the fact that our beam has finite power, we renormalize the intensity at each plane for better visibility of the results. We can see that the intensity profile, despite being noisy and seemingly random, repeats itself at those specific intervals.

Thus far we have discussed the Airy-Talbot effect in one transversal dimension, and the extension to two transversal

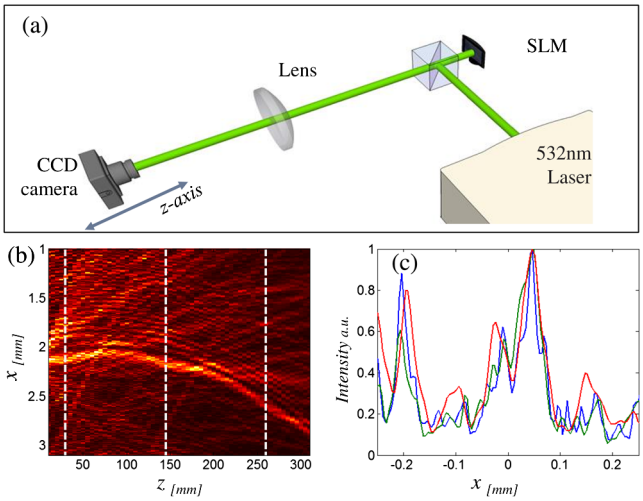

FIG. 2 (color online). Experimental realization of the Airy-Talbot effect. (a) Sketch of the experimental setup. (b) Intensity plot in the xz plane of the beam exhibiting the Airy-Talbot effect. The beam was generated using a SLM, by imposing a periodic phase profile in addition to the cubic phase profile. (c) Intensity cross sections along three planes of self-imaging, marked by dashed lines in (b). In order to make the comparison clearer, the cross sections are shifted along the parabolic trajectory. In addition, the intensity was normalized to account for the intensity attenuation caused by residual diffraction broadening due to the finite aperture of the beam.

dimensions is in order. The fundamental accelerating beam can be generated using a separation of variables, by a multiplication of two Airy beams, one in each coordinate [16,17]. When choosing the accelerating trajectory to be $u - (s^2/2\sqrt{2}) = \text{const}$, we get

$$\psi(u,v,s) = \mathrm{Ai}\left(\frac{u+v}{\sqrt{2}} - \frac{1}{4}s^2\right)\mathrm{Ai}\left(\frac{u-v}{\sqrt{2}} - \frac{1}{4}s^2\right) \times \exp\left(-\frac{1}{6}is^3 + \frac{1}{\sqrt{2}}us\right). \tag{11}$$

If we want to follow the same prescription as in the one-dimensional case, we essentially have two options: shift the solution in Eq. (11) along the u direction, or along the v direction. By looking at the phase factor in Eq. (11), we see that by summing different solutions, shifted at constant intervals Δ in u, we will get accelerating self-imaging at intervals along s that are equal to $\Gamma = (2\sqrt{2}\pi/\Delta)$. This is a direct analogue to the one-dimensional case discussed above. However, shifting in the v direction yields different results. Since the phase factor in Eq. (11) does not include v, adding shifted solutions does not change the self-similarity property at all, meaning that adding solutions that are shifted arbitrarily in v maintains the self-similarity property of Eq. (11) for all s values, and not only at constant intervals. Mathematically, summing solutions along v with a continuous spread of allowed shift values can be written as

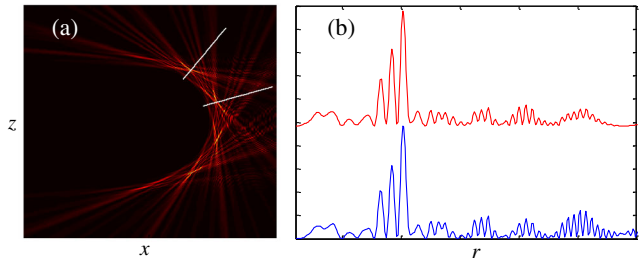

FIG. 3 (color online). (a) Intensity pattern arising from the sum of 20 nonparaxial half-Bessel-function beams with random coefficients. The nonparaxial, seemingly random field self-reproduces periodically with period $\pi/10$. Dashed lines mark two angles of self-imaging. (b) Intensity profile at cross sections defined by the dashed lines in (a).

$$\psi(u,v,0)=\int f(\beta)\mathrm{Ai}\left(\frac{u+(v-\beta)}{\sqrt{2}}\right)\mathrm{Ai}\left(\frac{u-(v-\beta)}{\sqrt{2}}\right)d\beta, \tag{12}$$

where $f(\beta)$ is an arbitrary function. Thus, any arbitrary wave form, given by the function $f(\beta)$ and Eq. (12), will be self-similar along a curved trajectory, for any s. The result in Eq. (12) is identical to the main result of Ref. [30].

Finally, we proceed to a theoretical examination of accelerating self-imaging under nonparaxial conditions. Accelerating solutions of Maxwell's equations were discovered in Ref. [25], and are written as "half-Bessel-functions" $J_\alpha^+(kx,kz)$, where k is the wave number and α is the integer order of the Bessel function. Writing our field as a sum of $J_\alpha^+(kx,kz)$ with different α values at constant intervals and arbitrary coefficients yields a function that is periodic in the angle $\theta=\arctan(z/x)$. As such, because the beam's maximal bending angle is 180°, the self-imaging will persist only a finite number of times. An example is presented in Fig. 3, where half-Bessel-function solutions with α ranging from 450 to 650 are added, with random coefficients. In Fig. 3(a) the intensity pattern in the x-z plane is plotted. In this case, the period is $\theta=\pi/10$. The two dashed lines in Fig. 3(a) mark two angles along which the intensity pattern self-images. The intensity along these lines is plotted in Fig. 3(b), where it can be clearly seen that the intensity self-images at those angles. Note that in the nonparaxial regime self-imaging is not perfect due to the fact that the self-similarity of the fundamental accelerating beam, the half-Bessel-function, is not perfect [25].

In conclusion, we have presented self-imaging along curved trajectories. That is, self-accelerating beams that self-reproduce periodically, in spite of the fact that the field is not necessarily periodic or the fact that it does not consist entirely of discrete values of propagation constants. In the paraxial regime, these wave packets are designed by adding shifted copies of the fundamental accelerating beam, with arbitrary coefficients. The arbitrary intensity distribution is then defined by the shift period and by a set of arbitrary coefficients. We have shown this effect theoretically and experimentally, and have discussed the generalization to higher dimensions and to nonparaxial propagation. Finally, we note that it is readily possible to generailize this effect to fields that accelerate along other trajectories, for example, elliptic ones, etc. [28,32,33]. This Airy-Talbot effect provides a deeper insight into the subject of accelerating and self-similar beams, and can be used as an improvement to optical testing techniques that use the Talbot effect. Likewise, the effect can be used in florescence microscopy, in the spirit of Ref. [21], to facilitate multiple excitations simultaneously. We thank Y. Plotnik for fruitful discussions. This work was supported by the ICORE Israeli Center of Excellence "Circle of Light", the Israel Science Foundation, and the Binational USA-Israel Science Foundation.

[1] H. F. Talbot, Philos. Mag. **9**, 401 (1836).
[2] Lord Rayleigh, Philos. Mag. **11**, 196 (1881).
[3] K. Patorski, Prog. Opt. **27**, 1 (1989).
[4] H. Ramezani, D. N. Christodoulides, V. Kovanis, I. Vitebskiy, and T. Kottos, Phys. Rev. Lett. **109**, 033902 (2012).
[5] K.-H. Luo, J. Wen, X.-H. Chen, Q. Liu, M. Xiao, and L.-A. Wu, Phys. Rev. A **80**, 043820 (2009).
[6] R. Iwanow, D. May-Arrioja, D. Christodoulides, G. Stegeman, Y. Min, and W. Sohler, Phys. Rev. Lett. **95**, 053902 (2005).
[7] E. Lau, Ann. Phys. (Berlin) **6**, 417 (1948).
[8] M. S. Chapman, C. R. Ekstrom, T. D. Hammond, J. Schmiedmayer, B. E. Tannian, S. Wehinger, and D. E. Pritchard, Phys. Rev. A **51**, R14 (1995).
[9] L. Deng, E. W. Hagley, J. Denschlag, J. E. Simsarian, M. Edwards, C. W. Clark, K. Helmerson, S. L. Rolston, and W. D. Phillips, Phys. Rev. Lett. **83**, 5407 (1999).
[10] W. Zhang, C. Zhao, J. Wang, and J. Zhang, Opt. Express **17**, 19757 (2009).
[11] F. Pfeiffer, M. Bech, O. Bunk, P. Kraft, E. F. Eikenberry, C. Brönnimann, C. Grünzweig, and C. David, Nat. Mater. **7**, 134 (2008).
[12] J. Turunen, A. Vasara, and A. T. Friberg, J. Opt. Soc. Am. A **8**, 282 (1991).
[13] T. Saastamoinen, J. Tervo, P. Vahimaa, and J. Turunen, J. Opt. Soc. Am. A **21**, 1424 (2004).
[14] J. Wen, Y. Zhang, and M. Xiao, Adv. Opt. Photonics **5**, 83 (2013).
[15] M. V. Berry and N. L. Balazs, Am. J. Phys. **47**, 264 (1979).
[16] G. A. Siviloglou and D. N. Christodoulides, Opt. Lett. **32**, 979 (2007).
[17] G. A. Siviloglou, J. Broky, A. Dogariu, and D. N. Christodoulides, Phys. Rev. Lett. **99**, 213901 (2007).
[18] M. A. Bandres, I. Kaminer, M. Mills, B. M. Rodríguez-Lara, E. Greenfield, M. Segev, and D. N. Christodoulides, Opt. Photonics News **24**, 30 (2013).
[19] J. Baumgartl, M. Mazilu, and K. Dholakia, Nat. Photonics **2**, 675 (2008).
[20] R. Schley, I. Kaminer, E. Greenfield, R. Bekenstein, Y. Lumer, and M. Segev, Nat. Commun. **5**, 5189 (2014).
[21] S. Jia, J. C. Vaughan, and X. Zhuang, Nat. Photonics **8**, 302 (2014).

[22] T. Vettenburg, H. I. C. Dalgarno, J. Nylk, C. Coll-Lladó, D. E. K. Ferrier, T. Čižmár, F. J. Gunn-Moore, and K. Dholakia, Nat. Methods **11**, 541 (2014).
[23] A. Chong, W. H. Renninger, D. N. Christodoulides, and F. W. Wise, Nat. Photonics **4**, 103 (2010).
[24] D. Abdollahpour, S. Suntsov, D. G. Papazoglou, and S. Tzortzakis, Phys. Rev. Lett. **105**, 253901 (2010).
[25] I. Kaminer, R. Bekenstein, J. Nemirovsky, and M. Segev, Phys. Rev. Lett. **108**, 163901 (2012).
[26] F. Courvoisier, A. Mathis, L. Froehly, R. Giust, L. Furfaro, P. A. Lacourt, M. Jacquot, and J. M. Dudley, Opt. Lett. **37**, 1736 (2012).
[27] P. Zhang, Y. Hu, D. Cannan, A. Salandrino, T. Li, R. Morandotti, X. Zhang, and Z. Chen, Opt. Lett. **37**, 2820 (2012).
[28] I. Kaminer, E. Greenfield, R. Bekenstein, J. Nemirovsky, A. Mathis, L. Froehly, F. Courvoisier, and M. Segev, Opt. Photonics News **23**, 26 (2012).
[29] N. Voloch-Bloch, Y. Lereah, Y. Lilach, A. Gover, and A. Arie, Nature (London) **494**, 331 (2013).
[30] M. A. Bandres, Opt. Lett. **34**, 3791 (2009).
[31] I. Kaminer, M. Segev, and D. N. Christodoulides, Phys. Rev. Lett. **106**, 213903 (2011).
[32] P. Aleahmad, M.-A. Miri, M. S. Mills, I. Kaminer, M. Segev, and D. N. Christodoulides, Phys. Rev. Lett. **109**, 203902 (2012).
[33] M. A. Bandres and B. M. Rodríguez-Lara, New J. Phys. **15**, 013054 (2013).